This article was downloaded by:
On: *14 January 2011*
Access details: *Access Details: Free Access*
Publisher *Taylor & Francis*
Informa Ltd Registered in England and Wales Registered Number: 1072954 Registered office: Mortimer House, 37-41 Mortimer Street, London W1T 3JH, UK

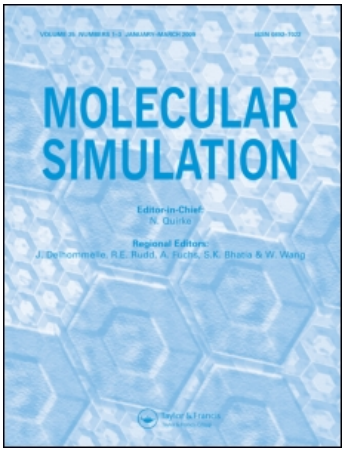

Molecular Simulation
Publication details, including instructions for authors and subscription information:
http://www.informaworld.com/smpp/title~content=t713644482

Assessing how metal-carbon interactions affect the structure of supported platinum nanoparticles

Brian H. Morrow[a]; Alberto Striolo[a]
[a] School of Chemical Biological and Materials Engineering, The University of Oklahoma, Norman, OK, USA

To cite this Article Morrow, Brian H. and Striolo, Alberto(2009) 'Assessing how metal-carbon interactions affect the structure of supported platinum nanoparticles', Molecular Simulation, 35: 10, 795 — 803
To link to this Article: DOI: 10.1080/08927020902787812
URL: http://dx.doi.org/10.1080/08927020902787812

PLEASE SCROLL DOWN FOR ARTICLE

Full terms and conditions of use: http://www.informaworld.com/terms-and-conditions-of-access.pdf

This article may be used for research, teaching and private study purposes. Any substantial or systematic reproduction, re-distribution, re-selling, loan or sub-licensing, systematic supply or distribution in any form to anyone is expressly forbidden.

The publisher does not give any warranty express or implied or make any representation that the contents will be complete or accurate or up to date. The accuracy of any instructions, formulae and drug doses should be independently verified with primary sources. The publisher shall not be liable for any loss, actions, claims, proceedings, demand or costs or damages whatsoever or howsoever caused arising directly or indirectly in connection with or arising out of the use of this material.

Molecular Simulation
Vol. 35, Nos. 10–11, September 2009, 795–803

Taylor & Francis
Taylor & Francis Group

Assessing how metal–carbon interactions affect the structure of supported platinum nanoparticles

Brian H. Morrow and Alberto Striolo*

School of Chemical Biological and Materials Engineering, The University of Oklahoma, Norman, OK 73019, USA

(*Received 19 December 2008; final version received 26 January 2009*)

Towards understanding the effect of solid supports on the catalytic activity of supported metal nanoparticles, all-atom molecular dynamics (MD) simulations are often conducted. However, these calculations are hampered by the uncertainty related to describing metal–support interactions (typically described as Lennard-Jones (LJ) potentials) at the atomic length scale. *Ab initio* electron-structure calculations are expected to refine such calculations by providing better estimates for the metal–support pair interaction potential. In the case of platinum nanoparticles supported on graphite, recent *ab initio* results suggest the correct energetic LJ parameter should be about four times that used in previous simulation studies from our group, as well as from others. Stimulated by these findings, MD simulations have been used here to investigate the effect of the magnitude of the metal–carbon interaction on the structure of supported metal nanoparticles. The LJ potential was used to model the metal–carbon interactions, and the embedded-atom method was used to model the metal–metal interactions. The morphology of platinum nanoparticles of 130, 249 and 498 atoms supported on graphite and various bundles of carbon nanotubes (CNTs) was studied. For the larger nanoparticle it was found that, although the details of platinum–carbon interactions are important for correctly capturing the morphological details, the morphology of the support is the primary factor that determines such features. Platinum–carbon interactions affect more significantly the results obtained for metal nanoparticles supported by CNT bundles. In this case, we found that the deviations become significant for small supported nanoparticles, as well as for nanoparticles of any size supported on CNTs of small diameter.

Keywords: molecular dynamics; metal nanoparticles

Downloaded At: 17:18 14 January 2011

1. Introduction

Supported metal nanoparticles are used in a wide variety of applications, including nanoelectronics, nanosensing and catalysis. In catalysis, metal nanoparticles, often platinum, are used in such reactions as selective hydrogenation [1], oxidation of formic acid and formaldehyde [2], and, perhaps most notably, in reactions such as oxygen reduction that occur in fuel cells [3–5]. Often these nanoparticles are supported by carbon-based materials such as graphite or carbon nanotubes (CNTs). The interaction between the metal and the support is important, as it affects the structure and thus the catalytic activity of the metal. Weak interactions may lead to sintering and, consequently, increased nanoparticle size. Density functional theory (DFT) can be used to study such interactions [6,7], but these calculations are limited to small systems containing tens of metal atoms, rather than the hundreds to thousands of atoms typically found in catalytic nanoparticles. *Ab initio* molecular dynamics (MD) can be used to study the behaviour of these systems over time, although due to computational demands the timescale accessible by these simulations is limited. MD simulations can be used to study large nanoparticles at any temperature, and can yield dynamic properties. For example, we used MD simulations to study the structure and diffusion of platinum nanoparticles of 130, 249 and 498 atoms supported by graphite and different types of CNTs [8,9]. Many other MD studies of supported metal nanoparticles can be found in the literature [10–24]. One drawback to these simulations is that there is no well-established potential for modelling the interaction of the metal with the carbon support. A simple Lennard-Jones (LJ) potential is commonly used, often with parameters obtained from MD simulations of pure compounds (metals and carbon supports) according to the Lorentz–Berthelot mixing rules. Alternatively, the parameters could be obtained from *ab initio* electron-structure calculations. A recent study by Acharya et al. [25] used DFT to parameterise an LJ potential between carbon atoms in graphite and one platinum atom, obtaining a value for the LJ energy parameter, ε, approximately four times higher than those previously used. Other previous DFT studies for Pt adsorption on CNTs [26] revealed that the adsorption energy increases as the curvature of the support increases, almost according to a linear dependency. This suggests that the ε used to describe Pt–C interactions should increase as the CNT diameter decreases. In this report, we have used the potential of Acharya et al., modified to account for the curvature of the support, to study how the

*Corresponding author. Email: astriolo@ou.edu

ISSN 0892-7022 print/ISSN 1029-0435 online
© 2009 Taylor & Francis
DOI: 10.1080/08927020902787812
http://www.informaworld.com

Pt–C interactions affect the structure of platinum nanoparticles supported by graphite and CNTs.

2. Computational details

Calculations were performed using the large-scale atomic/molecular massively parallel simulator (LAMMPS) [27]. All simulations were performed in the NVT ensemble (constant number of particles N, simulation box volume V and temperature T). Because we expect that the results, in terms of qualitative comparison between the morphology of the supported metal nanoparticles obtained by implementing different force fields, will not depend significantly on the simulation temperature, the simulations were conducted at 700 K, a temperature high enough to allow fast atomic mobility, but below the melting temperature of the nanoparticle. Furthermore, our previous simulations indicate that the structure of the supported metal nanoparticle does not change significantly as the temperature decreases below 700 K. Similar observations are expected within the range of Pt–C interaction potentials considered herein.

Periodic boundary conditions were used in all simulations. The embedded-atom method (EAM) [28], which has been used to successfully model the properties of both free and supported metal nanoparticles [29–31], was used to model platinum–platinum interactions. In the EAM model, the total potential energy is given by

$$U = \sum_i F_i\left(\sum_{j\neq i}\rho_j(r_{ij})\right) + \frac{1}{2}\sum_i\sum_{j\neq i}\phi_{ij}(r_{ij}), \qquad (1)$$

where $F_i(\rho)$ is the energy required to embed atom i into the background electron density, ρ_j is the electron density due to atom j and $\phi_{ij}(r_{ij})$ is the repulsion between the cores of atoms i and j separated by a distance r_{ij}. The force field parameters used to model platinum are those developed by Foiles et al. [28] as included in the Pt_u3.eam potential file in the LAMMPS package. The cut-off distance for Pt–Pt interactions is set to 5.3 Å. The simulation procedure is described at length in our previous manuscript [8]. The platinum–carbon interactions were modelled using the 12-6 LJ potential:

$$E(r_{ij}) = 4\varepsilon_{ij}\left[\left(\frac{\sigma_{ij}}{r_{ij}}\right)^{12} - \left(\frac{\sigma_{ij}}{r_{ij}}\right)^{6}\right]. \qquad (2)$$

The parameter ε_{ij} has units of energy and indicates how strongly atoms i and j are attracted, while σ_{ij} has units of length and is related to the size of atoms i and j. We have used four different sets of LJ parameters in our simulations. The first set was used in our previous work [8,9] and that of others [13,14,32]. The parameters were derived [15,33] by simulating pure platinum using the Sutton–Chen many-body potential [34], and then fitting the LJ parameters to these results. The Pt–C parameters were then obtained from the Pt–Pt ones using C–C parameters and the Lorentz–Berthelot mixing rules [35]. These parameters, referred to in the text below as potential 1, are $\varepsilon_1 = 0.02206$ eV and $\sigma_1 = 2.95$ Å. The second set of parameters was obtained by Acharya et al. [25], who performed DFT calculations to determine the binding energy of one Pt atom at various sites on graphite. The data were used to generate a potential energy surface, which was reproduced by appropriately fit LJ parameters. In order to match the DFT results, ghost atoms with zero mass were introduced in the centre of the hexagonal carbon rings in graphite. According to this parameterisation, referred to in the text below as potential 2, the LJ parameters are $\varepsilon_2 = 0.09$ eV and $\sigma_2 = 1.60$ Å for the carbon atoms and $\varepsilon_g = 0.25$ eV and $\sigma_g = 2.20$ Å for the ghost atoms. In all simulations conducted below for nanoparticles supported on graphite, a single graphene sheet is used. When potential 2 is used, ghost atoms are inserted in the centre of the hexagonal rings.

Bundles of (4,4) and (10,10) CNTs were also considered as substrates. DFT simulations by Chi et al. [26] have shown that the binding energy of an adsorbed platinum atom increases with the curvature of the graphene substrate. For example, on a flat graphene sheet (curvature of 0 $Å^{-1}$) Chi et al. found a binding energy of 1.45 eV, while on a (10,10) CNT (curvature of ~ 0.147 $Å^{-1}$) the binding energy increases to ~ 2.28 eV. Therefore, the smaller the nanotube, the higher the binding energy is. We mimic this effect by scaling ε_2 when Pt nanoparticles are supported on CNTs. The ratio of the binding energy of platinum on (10,10) CNTs to platinum on graphite, as calculated by Chi et al., is 1.517, so ε_2 was multiplied by this factor for the simulations on (10,10) CNTs. This potential is referred to in the text as potential 3. The (4,4) CNTs, which we have used in previous simulations, were not included in the work of Chi et al. Assuming a linear extrapolation of the binding energy versus curvature graph, we estimated the binding energy of Pt on (4,4) CNTs to be 2.07 times that on graphite and the ε parameter was scaled accordingly. This potential is referred to as potential 4. We caution that these factors are

Table 1. Summary of LJ parameters used to describe Pt–C pair interactions.

	ε (eV)	σ (Å)
Potential 1	0.02206	2.95
Potential 2	0.09	1.60
Potential 3	0.1365	1.60
Potential 4	0.1863	1.60

Downloaded At: 17:18 14 January 2011

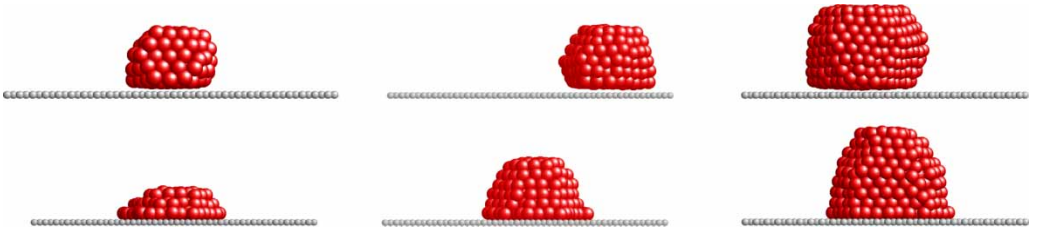

Figure 1. Simulation snapshots obtained at 700 K for Pt_{130} (left), Pt_{249} (centre) and Pt_{498} (right). Platinum atoms are red, carbon atoms are gray (colour online). Snapshots obtained using potential 1 are on the top; those obtained using potential 2 are on the bottom.

approximate and are only used to qualitatively study the effect of curvature on the structure of supported metal nanoparticles; in fact, DFT-derived force fields are not available for Pt atoms on CNTs. For this reason, it is not possible to implement the force fields by describing 'ghost' atoms, as was done in the case of graphite. The four sets of LJ parameters used here [two for graphite, one of (4,4) CNTs and one for (10,10) CNTS] are summarised in Table 1.

3. Results and discussion

3.1 Nanoparticles on graphite

Sample simulation snapshots for Pt_{130}, Pt_{249} and Pt_{498} on graphite at 700 K are reported in Figure 1, with the results obtained using potential 1 on the top and those obtained using potential 2 on the bottom. The most obvious difference occurs in the structure of Pt_{130}, in which case potential 2 causes the nanoparticle to flatten and spread out, while potential 1 allows the nanoparticle to maintain

Downloaded At: 17:18 14 January 2011

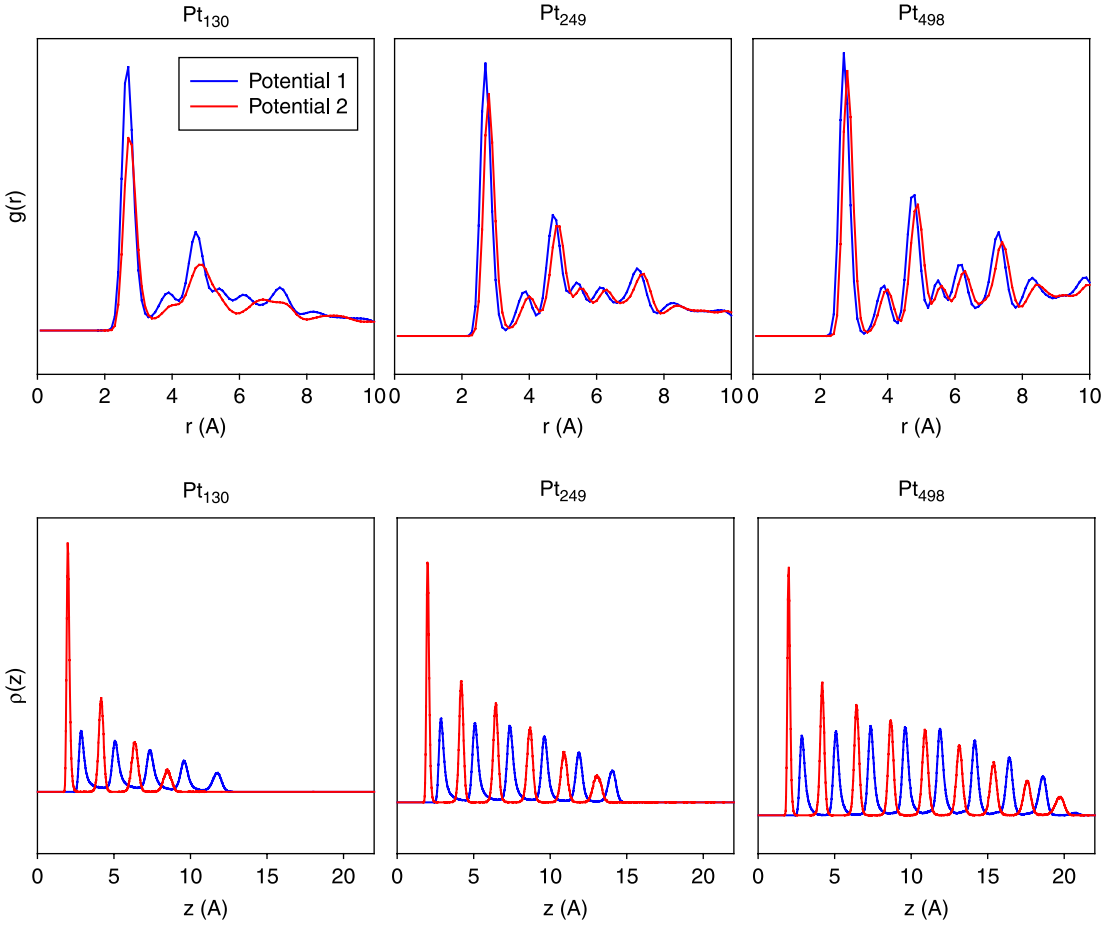

Figure 2. Radial distribution functions (top) and density profiles (bottom) for Pt_{130} (left), Pt_{249} (centre) and Pt_{498} (right). Results obtained using potential 1 are shown in blue; those obtained using potential 2 are shown in red (colour online).

a more spherical structure. As the particle becomes larger, the change due to the different potentials becomes less pronounced, although the contact angle appears smaller when potential 2 is used. In the case of both Pt_{249} and Pt_{498}, when potential 2 is implemented the nanoparticles show a somewhat pyramidal shape. The base is wide and the nanoparticle width decreases, to some extent, farther from the graphite sheet.

These changes to the nanoparticle morphology were quantified by calculating a radial distribution function [35], *g(r)*, for atoms within 5 Å of the nanoparticle's centre of mass, as well as by density profiles along the *z*-axis (perpendicular to the graphite sheet). These results, averaged over one 7.5 ns-long simulation run at 700 K, are reported in Figure 2. For all three particle sizes, the radial distribution functions obtained with the two potentials are similar, with the large peaks occurring at the same distances from the centre. For Pt_{249} and Pt_{498} the radial distribution functions obtained using the two Pt–C potentials are very similar, with the positions of the intermediate peaks almost identical. In the case of Pt_{130} there are no intermediate peaks when potential 2 is used. To some extent, it appears that implementing potential 2 yields less structured nanoparticles for Pt_{130}. This observation is corroborated by the snapshots shown in Figure 1, which demonstrate how Pt_{130} undergoes a dramatic change when potential 1 was switched to potential 2. The differences in the density profiles away from graphite (Figure 2, bottom panels) reflect the differences in morphology shown in Figure 1 and discussed above. The features of the supported nanoparticles obtained implementing potential 1 are extensively discussed in our previous publications [8,9]. In the case of potential 2, because the nanoparticles assume a pyramidal structure (see Figure 1), the density profiles are consistent with the nanoparticles tapering, with peaks close to the surface enhanced and peaks farther from the surface decreased as compared to the density profile found using potential 1. The first peak in the density profiles is also shifted closer to the graphite sheet, since σ_2 is smaller than σ_1. The position of the first peak in the density profile, which is due to the carbon–platinum LJ size parameter, should in principle be accessible from experimental observation. Unfortunately, to the best of our knowledge, such information is not available. However, and most importantly, the distance between subsequent peaks in the

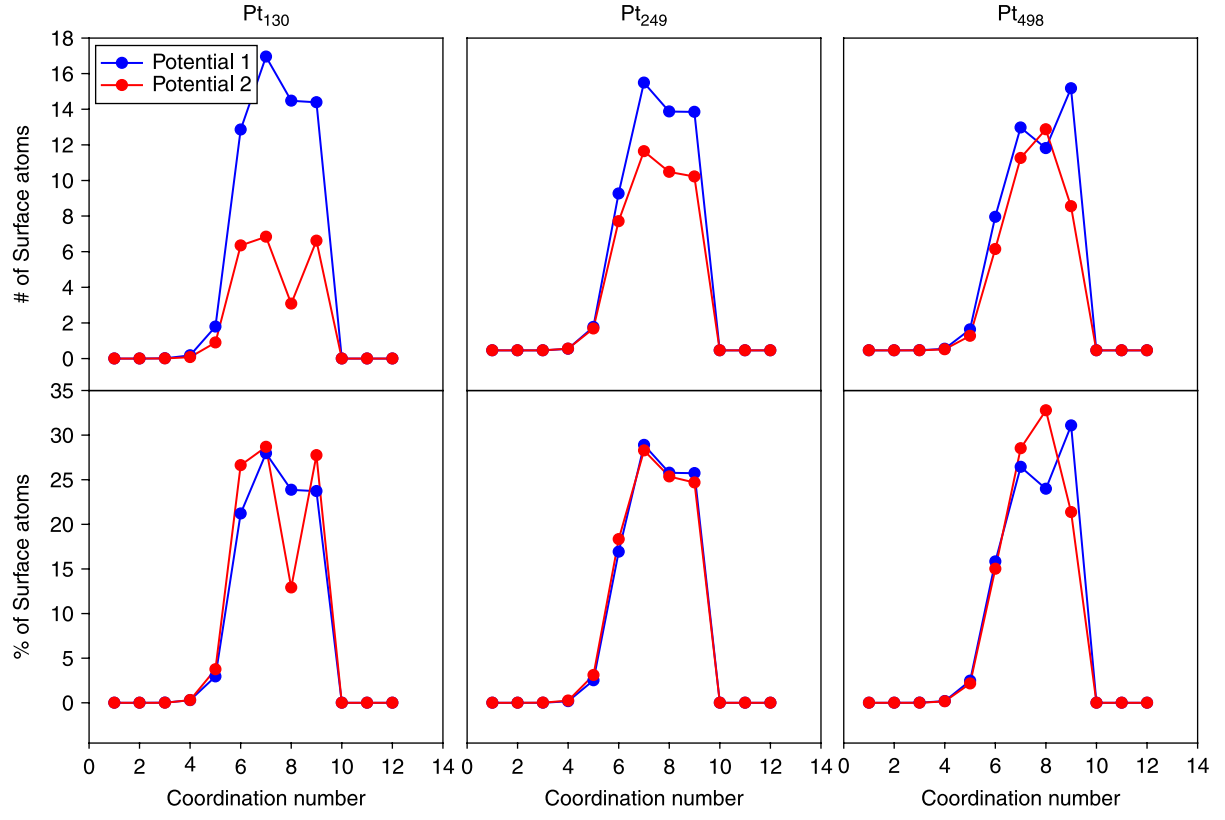

Figure 3. Number of surface atoms (top) and percentage of surface atoms (bottom) with a given coordination number for Pt_{130} (left), Pt_{249} (centre) and Pt_{498} (right) on graphite. Results obtained using potential 1 are shown in blue; those obtained using potential 2 are shown in red (colour online).

Downloaded At: 17:18 14 January 2011

density profiles of Figure 2 using both potentials is identical, indicating that the Pt–Pt interactions are strong enough to maintain the crystal structure of the platinum within the nanoparticles despite the increased Pt–C interactions.

To further characterise the nanoparticles' structure, we calculated the coordination numbers of the surface platinum atoms. The coordination number of a given atom is defined as the number of neighbours within 3.1 Å of that atom. The number (top) and percentage (bottom) of surface atoms having a given coordination number are reported in Figure 3. Increasing the strength of the Pt–C interaction causes a decrease in the number of surface atoms. This is a direct consequence of the change in morphology of the supported nanoparticles, and therefore the effect is stronger for the smaller nanoparticles considered. However, the percentage of surface atoms having a given coordination number does not change significantly when different potentials are used to describe Pt–C interactions. The largest difference occurs for surface atoms in Pt_{130} with a coordination number of 8, which undergoes a decrease of about 10% when potential 1 is switched to potential 2.

3.2 *Nanoparticles on CNTs*

Additional simulations were performed for Pt_{249} supported by (4,4) and (10,10) CNTs. As described above, three sets

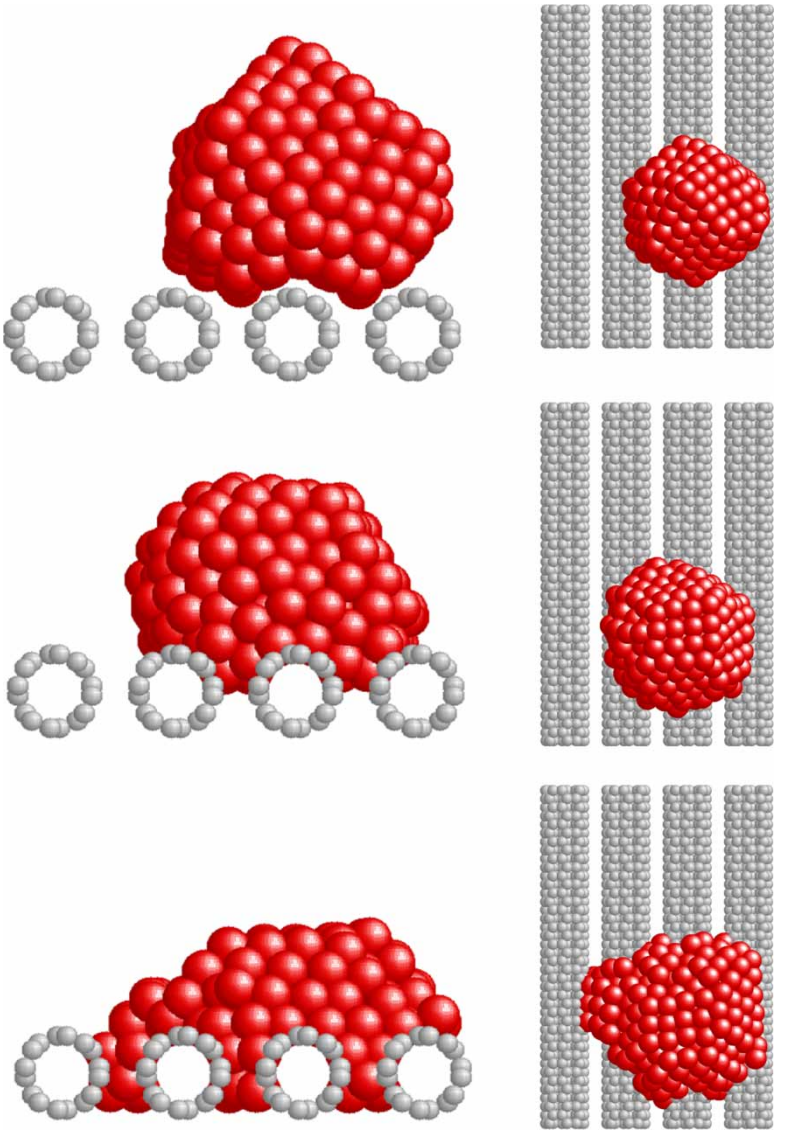

Figure 4. Side view (left) and top view (right) of simulation snapshots obtained at 700 K for Pt_{249} on (4,4) CNTs. Platinum atoms are red, carbon atoms are gray (colour online). Snapshots obtained using potential 1 are on the top, snapshots obtained using potential 2 are in the middle and snapshots obtained using potential 4 are on the bottom.

Downloaded At: 17:18 14 January 2011

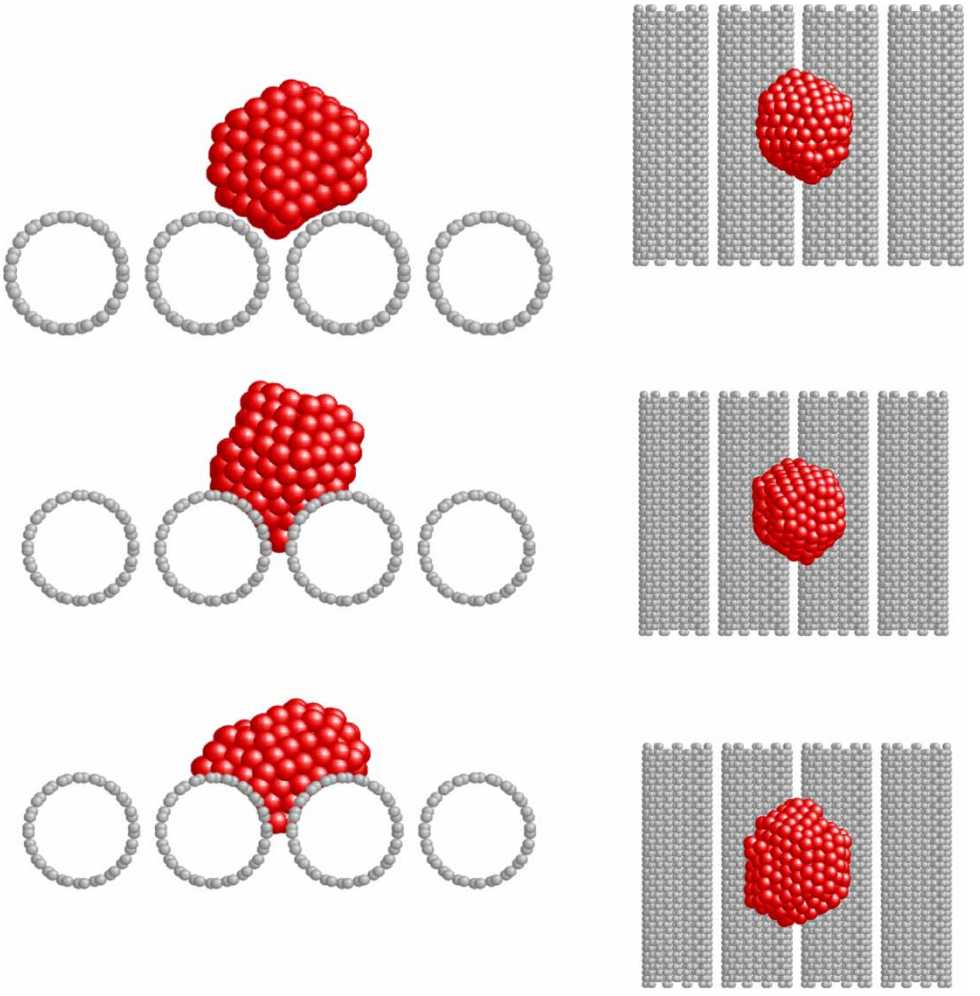

Figure 5. Side view (left) and top view (right) of simulation snapshots obtained at 700 K for Pt_{249} on (10,10) CNTs. Platinum atoms are red, carbon atoms are gray (colour online). Snapshots obtained using potential 1 are on the top, snapshots obtained using potential 2 are in the middle and snapshots obtained using potential 3 are on the bottom.

Downloaded At: 17:18 14 January 2011

of LJ potentials were used for the Pt–C interactions: the base-case potential 1, the DFT-derived potential 2 and potentials 3 and 4, which account for the curvature of the CNTs. Snapshots obtained at 700 K are shown in Figures 4 and 5, with potential 1 on top, potential 2 in the middle and potentials 3 or 4 on the bottom. To clarify the following comments, we point out that the ε parameter increases from potential 1, to potentials 2–4. As observed on graphite, as the LJ ε parameter increases the base of the nanoparticle near the support becomes wider. In addition, when large ε values are used Pt atoms are pulled between the nanotubes, with this effect becoming more pronounced using potential 4 (Figure 4, bottom panels), which is the most attractive potential considered here.

We quantified the simulation results summarised in Figures 4 and 5 using radial distribution functions and density profiles perpendicular to the substrate, as reported in Figure 6. For all Pt–C potentials considered the radial distribution functions are similar, with only three prominent peaks, and only minor differences in peak intensity and location. This is quite surprising given the large differences in morphologies discussed above, but is consistent with the fact that Pt–Pt interactions predominantly determine the arrangement of metal atoms near the nanoparticle centre of mass.

Differences between the simulation results are more evident when the density profiles are compared. The profiles calculated using potentials 1 and 2 do not exactly match, but the peaks have similar locations and intensities. The profiles calculated using potential 2 and potential 3 or 4 have peaks in the same location at distances below ~ 10 Å, although the peaks are more intense when potential 3 or 4 is used. It appears that the effect of accounting for nanotube curvature within the Pt–C interaction becomes significant for nanoparticles supported on (4,4) CNTs, but is not dramatic for nanoparticles on (10,10) CNTs, although in

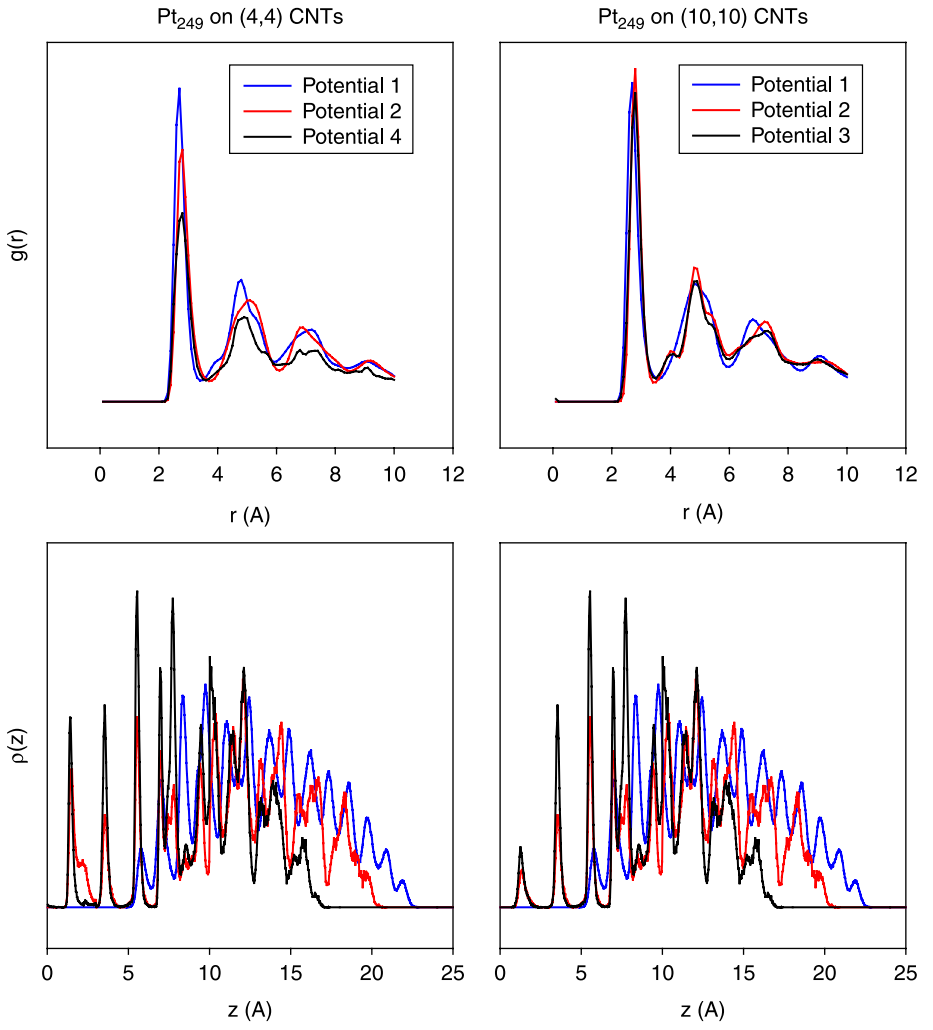

Figure 6. Radial distribution functions (top) and density profiles (bottom) for Pt_{249} on (4,4) CNTs (left) and (10,10) CNTs (right). Results obtained using potential 1 are shown in blue, results obtained using potential 2 are shown in red and results obtained using potential 3 (right) or 4 (left) are shown in black (colour online).

both cases the nanoparticles are more 'flat' when potential 3 or 4 is implemented.

The differences and similarities between the platinum nanoparticles on graphite and CNTs should also be examined. For both potentials, Pt on graphite has regular density profiles, with evenly spaced peaks. On CNTs, the density profiles are much more disordered, with many smaller irregular peaks, because of the structural change caused by the curvature of the nanotube. These disordered density profiles are observed independently of which Pt–C potential is implemented. The differences between the density profiles on graphite and CNTs are indicative of a change in the nanoparticle structure primarily due to the geometry of the support. These structural changes are captured by both potentials, indicating that either would be suitable for a qualitative investigation of the structure of supported metal nanoparticles. However, our results suggest that when small nanoparticles are simulated and/or when the nanoparticles are supported on CNTs of small diameter (large curvature) the details of the force fields do affect the simulation results significantly, and therefore, not surprisingly, the most accurate force fields available should be implemented when all-atom MD simulations are performed.

To complete the analysis of our comparative study we calculated the number and percentage of surface atoms with a given coordination number, reported in Figure 7. As was observed for nanoparticles on graphite, increasing the strength of the Pt–C interaction decreases the number of surface atoms, with nanoparticles simulated with potential 1 having the most surface atoms and those simulated with potential 3 or 4 having the least. However, the percentage of surface atoms having a given coordination number remains almost identical in all cases considered. In this case, the largest difference is about 5% for atoms on the (4,4) CNTs with coordination

Downloaded At: 17:18 14 January 2011

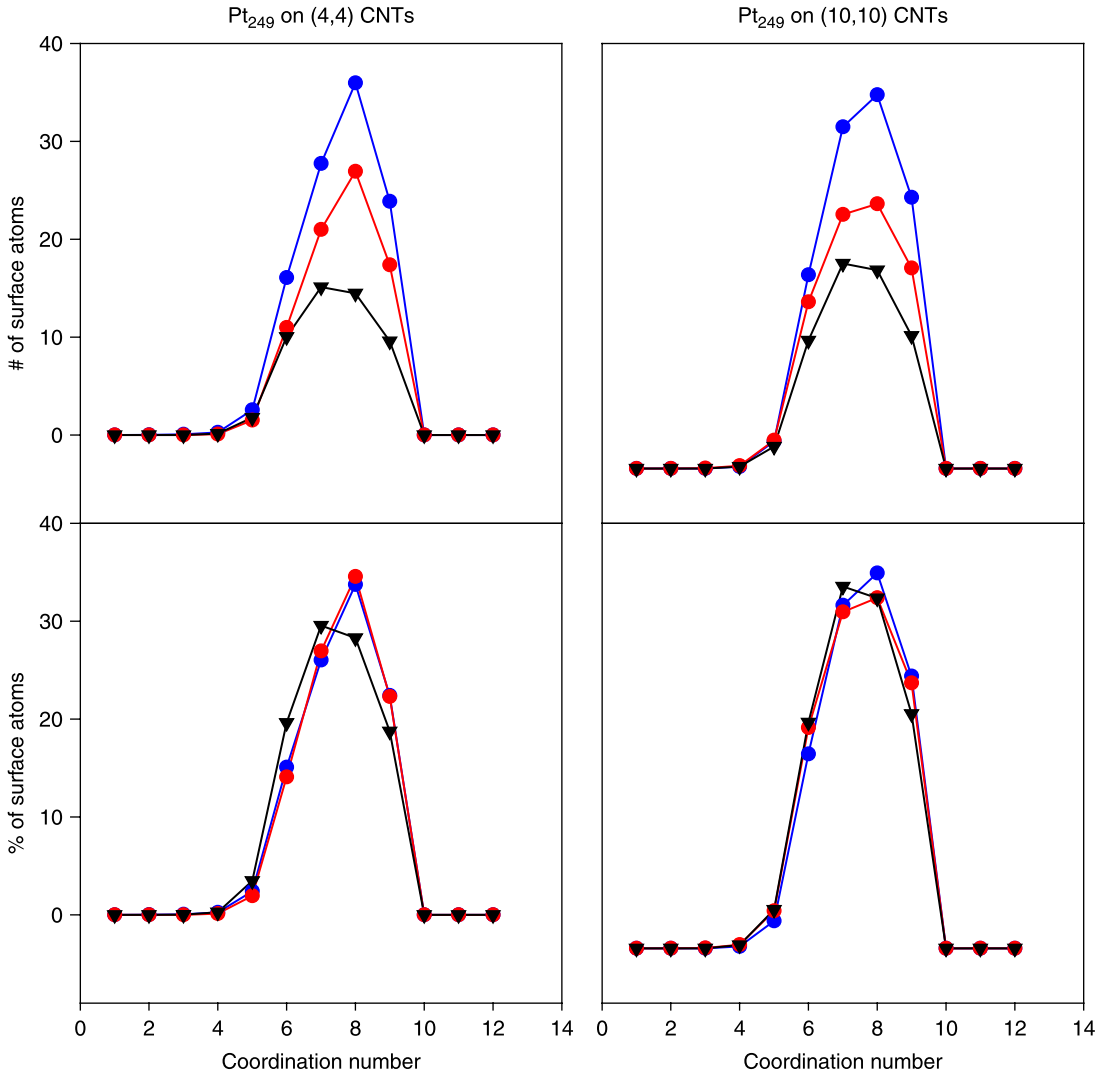

Figure 7. Number of surface atoms (top) and percentage of surface atoms (bottom) having the given coordination number for Pt_{249} on (4,4) CNTs (left) and (10,10) CNTs (right). Results obtained using potential 1 are shown in blue, results obtained using potential 2 are shown in red and results obtained using potential 3 (right) or 4 (left) are shown in black (colour online).

number 8. It is expected that the differences will become smaller as the nanoparticles size increases. This latter result is encouraging when simulations such as those presented here are conducted within the field of catalysis, in which case the coordination numbers of the surface metal atoms are expected to strongly affect the catalytic activity of supported metal nanoparticles.

4. Conclusions

MD simulations were conducted for platinum nanoparticles supported on carbonaceous materials at 700 K. The results were compared when four sets of parameters were implemented to describe the metal–carbon LJ interactions. Potential 1, taken from literature, had been derived using MD, while potential 2 had been derived using DFT. Potentials 3 and 4 were obtained by modifying potential 2 to account for the effect of the curvature of the carbon support. The value of the LJ energetic parameter ε is approximately four times higher in potential 2 than in potential 1, which has been used in several previous simulations. The parameter ε further increases in potentials 3 and 4.

As expected, our calculations show that implementing different potentials to describe metal–carbon interactions quantitatively affects the results. Thus, when possible, the most accurate potentials should be used, especially when small (less than $\sim$200 atoms) metal nanoparticles are simulated. However, limited to the conditions considered in this work, our results, expressed in terms of the density

Downloaded At: 17:18 14 January 2011

profiles of Pt atoms perpendicular to the support, radial distribution function around the metal atoms near the nanoparticles' centre of mass and number and percentage of surface metal atoms on the supported metal nanoparticles with given coordination number, do not show dramatic differences when different force fields are implemented to describe Pt–C interactions. This observation suggests that the geometry of the carbon support (i.e. flat graphite vs. curved nanotubes) is the predominant factor that affects the morphology of the supported nanoparticle, and in particular the coordination number of the metal atoms on their surfaces.

Acknowledgements

The authors acknowledge financial support from the US DOE under contract #FG02-06ER64239, and from the Vice President for Research at the University of Oklahoma through a Junior Faculty Research Program award. Generous allocations of computing time were provided by the OU Supercomputing Center for Education and Research (OSCER) at the University of Oklahoma and by the National Energy Research Scientific Computing Center (NERSC) at Lawrence Berkeley National Laboratory.

Downloaded At: 17:18 14 January 2011

References

[1] J.-P. Tessonnier, L. Pesant, G. Ehret, M.J. Ledoux, and C. Pham-Huu, *Pd nanoparticles introduced inside multi-walled carbon nanotubes for selective hydrogenation of cinnamaldehyde into hydrocinnamaldehyde*, Appl. Catal. A 288 (2005), pp. 203–210.

[2] V. Selvaraj, M. Alagar, and K.S. Kumar, *Synthesis and characterization of metal nanoparticles-decorated PPY–CNT composite and their electrocatalytic oxidation of formic acid and formaldehyde for fuel cell applications*, Appl. Catal. B 75 (2007), pp. 129–138.

[3] S.S. Gupta, N.R. Bandyopadhya, and J. Datta, *Carbon-supported platinum catalysts for direct alcohol fuel cell anode*, Mater. Manuf. Process. 21 (2006), pp. 703–709.

[4] W. Li, C. Liang, J. Qiu, W. Zhou, H. Han, Z. Wei, G. Sun, and Q. Xin, *Carbon nanotubes as support for cathode catalyst of a direct methanol fuel cell*, Carbon 40 (2002), pp. 791–794.

[5] S.H. Joo, S.J. Choi, I. Oh, J. Kwak, Z. Liu, O. Terasaki, and R. Ryoo, *Ordered nanoporous arrays of carbon supporting high dispersions of platinum nanoparticles*, Nature 412 (2001), p. 169.

[6] L.-L. Wang, S.V. Khare, V. Chirita, D.D. Johnson, A.A. Rockett, A.I. Frenkel, N.H. Mack, and R.G. Nuzzo, *Origin of bulklike structure and bond length disorder of Pt_{37} and Pt_6Ru_{37} clusters on carbon: Comparison of theory and experiment*, J. Am. Chem. Soc. 128 (2006), pp. 131–142.

[7] L.-L. Wang and D.D. Johnson, *Shear instabilities in metallic nanoparticles: Hydrogen-stabilized structure of Pt_{37} on carbon*, J. Am. Chem. Soc. 129 (2007), pp. 3658–3664.

[8] B.H. Morrow and A. Striolo, *Morphology and diffusion mechanism of platinum nanoparticles on carbon nanotube bundles*, J. Phys. Chem. C 111 (2007), pp. 17905–17913.

[9] B.H. Morrow and A. Striolo, *Platinum nanoparticles on carbonaceous materials: The effect of support geometry on nanoparticle mobility, morphology, and melting*, Nanotechnology 19 (2008), 195711.

[10] S.-P. Huang, D.S. Mainardi, and P.B. Balbuena, *Structure and dynamics of graphite-supported bimetallic nanoclusters*, Surf. Sci. 545 (2003), pp. 163–179.

[11] W.D. Luedtke and U. Landman, *Slip diffusion and Levy flights of an adsorbed gold nanocluster*, Phys. Rev. Lett. 82 (1999), pp. 3835–3838.

[12] L.J. Lewis, P. Jensen, N. Combe, and J.L. Barrat, *Diffusion of gold nanoclusters on graphite*, Phys. Rev. B 61 (2000), pp. 16084–16090.

[13] P. Jensen, A. Clement, and L.J. Lewis, *Diffusion of nanoclusters on non-ideal surfaces*, Physica E 21 (2004), pp. 71–76.

[14] S.-P. Huang and P.B. Balbuena, *Platinum nanoclusters on graphite substrates: A molecular dynamics study*, Mol. Phys. 100 (2002), pp. 2165–2174.

[15] S.Y. Liem and K.-Y. Chan, *Simulation study of platinum adsorption on graphite using the Sutton–Chen potential*, Surf. Sci. 328 (1995), pp. 119–128.

[16] G.-W. Wu and K.-Y. Chan, *Morphology of platinum clusters on graphite at different loadings*, Surf. Sci. 365 (1996), pp. 38–52.

[17] Z. Gu and P.B. Balbuena, *Structural characterization of Pt nanoclusters deposited on graphite: Effects of substrate and surrounding medium*, Catal. Today 105 (2005), pp. 152–161.

[18] J. Chen and K.-Y. Chan, *Size-dependent mobility of platinum cluster on a graphite surface*, Mol. Simul. 31 (2005), pp. 527–533.

[19] E.J. Lamas and P.B. Balbuena, *Adsorbate effects on structure and shape of supported nanoclusters: A molecular dynamics study*, J. Phys. Chem. B 107 (2003), pp. 11682–11689.

[20] S.K.R.S. Sankaranarayanan, V.R. Bhethanabotla, and B. Joseph, *Molecular dynamics simulations of the structural and dynamic properties of graphite-supported bimetallic transition metal clusters*, Phys. Rev. B 72 (2005), 195405.

[21] B. Yoon, W.D. Luedtke, J. Gao, and U. Landman, *Diffusion of gold clusters on defective graphite surfaces*, J. Phys. Chem. B 107 (2003), pp. 5882–5891.

[22] G.-W. Wu and K.-Y. Chan, *Molecular simulation of platinum clusters on graphite*, Surf. Rev. Lett. 4 (1997), pp. 855–858.

[23] G.-W. Wu and K.-Y. Chan, *Molecular simulation of oxygen on supported platinum clusters*, J. Electroanal. Chem. 450 (1998), pp. 225–231.

[24] S.H. Lee, S.S. Han, J.K. Kang, J.H. Ryu, and H.M. Lee, *Phase stability of Pt nanoclusters and the effect of a (0 0 0 1) graphite surface through molecular dynamics simulation*, Surf. Sci. 602 (2008), pp. 1433–1439.

[25] C.K. Acharya, D.I. Sullivan, and C.H. Turner, *Characterizing the interaction of Pt and PtRu clusters with boron-doped, nitrogen-doped, and activated carbon: DFT calculations and parameterization*, J. Phys. Chem. C 112 (2008), pp. 13607–13622.

[26] D.H. Chi, N.T. Cuong, N.A. Tuan, Y.-T. Kim, H.T. Bao, T. Mitani, T. Ozaki, and H. Nagao, *Electronic structures of Pt clusters adsorbed on (5,5) single wall carbon nanotube*, Chem. Phys. Lett. 432 (2006), pp. 213–217.

[27] S. Plimpton, *Fast parallel algorithms for short-range molecular dynamics*, J. Comp. Phys. 117 (1995), pp. 1–19.

[28] S.M. Foiles, M.I. Baskes, and M.S. Daw, *Embedded-atom-method functions for the fcc metals Cu, Ag, Au, Ni, Pd, Pt, and their alloys*, Phys. Rev. B 33 (1986), pp. 7983–7991.

[29] M.S. Daw, S.M. Foiles, and M.I. Baskes, *The embedded-atom method: A review of theory and applications*, Mater. Sci. Rep. 9 (1993), pp. 251–310.

[30] O.S. Trushin, P. Salo, and T. Ala-Nissila, *Energetics and many-particle mechanisms of two-dimensional cluster diffusion on Cu(100) surfaces*, Phys. Rev. B 62 (2000), pp. 1611–1614.

[31] A. Sebetci and Z.B. Güvenç, *Energetics and structures of small clusters: PtN,* $N = 2–21$, Surf. Sci. 525 (2003), pp. 66–84.

[32] J. Liu, M.E. Selvan, S. Cui, B.J. Edwards, D.J. Keffer, and W.V. Steele, *Molecular-level modeling of the structure and wetting of electrode/electrolyte interfaces in hydrogen fuel cells*, J. Phys. Chem. C 112 (2008), pp. 1985–1993.

[33] S.Y. Liem and K.-Y. Chan, *Effective pairwise potential for simulations of adsorbed platinum*, Mol. Phys. 86 (1995), pp. 939–949.

[34] A.P. Sutton and J. Chen, *Long-range Finnis–Sinclair potentials*, Philos. Mag. Lett. 61 (1990), pp. 139–146.

[35] M.P. Allen and D.J. Tildesley, *Computer Simulation of Liquids*, Oxford University Press, Oxford, 2004, pp. 24, 54–55.